Linear mapping of region-to-region connectivity as a basic principle of visual and prefrontal functional organization alike

Jonathan F. O'Rawe and Hoi-Chung Leung

Stony Brook University

Integrative Neuroscience Program, Department of Psychology

Abstract

The organization of region-to-region functional connectivity has major implications for understanding information transfer and transformation between brain regions. We extended connective field mapping to 3-dimensional anatomical space to derive estimates of cortico-cortical functional organization. Using multiple publicly available resting-state fMRI data samples for model testing and replication analysis, we have three main findings. First, we found that the topology of functional connectivity between early visual regions maintained a linear relationship along the anterior-posterior dimension, which corroborates previous research. Higher order visual regions such as the fusiform face area however, showed a pattern of connectivity that supports convergence and biased sampling, which seems to contribute to their core receptive field properties. Second, we demonstrated that linearity of input is a fundamental aspect of functional connectivity of the entire cortex, with higher linearity between regions within a functional network than across networks. The principle gradient of linearity across the cortex resembled the decompositions found in previous work using conventional functional connectivity analysis and models of cortical genetic expression. Last but not least, we showed that the linearity gradients in the lateral prefrontal cortex are partially accounted for by differential dorsal and ventral stream inputs as well as increasing convergence to anterior regions, which support the concurrence of the two main theoretical accounts of prefrontal organization: domain specialization and abstraction of information processing. In sum, these findings suggest that linearity of input is a fundamental motif of functional connectivity between cortical regions for information processing and transfer, with high linearity potentially important for preserving the integrity of information from one region to another within a functional network.

1. Introduction

One primary goal of systems neuroscience is to understand how integration occurs across cortical areas in order to support complex behavior (Cavada & Goldman-Rakic, 1991; Haber, Fudge, & McFarland, 2000; Hoover & Strick, 1993). As different brain regions display spatially specific patterns of long range and short range connections to their target regions (Kravitz, Saleem, Baker, & Mishkin, 2011; Kravitz, Saleem, Baker, Ungerleider, & Mishkin, 2013; Van Essen & Gallant, 1994), it is believed that the particular properties of brain circuitry must provide a foundation of brain function and information processing, and that connectivity profiles from one region to another allows for the potential understanding of information transfer/transformation. Topographic (linear), convergent, and divergent connectivity have been postulated to support different computational needs of a specific neural network (Thivierge & Marcus, 2007). For example, systematic convergent connectivity in the visual hierarchy has been shown to be responsible for object processing, from lines (Hubel & Wiesel, 1962) to complex objects (Tanaka, 1997), while divergent connectivity has been theorized in motor systems for complex feedback mechanisms, such as motor efference copies (Wolpert & Flanagan, 2001).

Neuroimaging studies of brain connectivity, while indirect, have the benefit of their exhaustive sampling across the entire anatomical space, which complement the interpretations from the sparse sampling of rigorous anatomical tracing in animals. This is evident in functional connectivity studies using resting state fMRI data, from which a low dimensional structure of large scale networks has been consistently observed as a key organizational feature of the cortex (Biswal et al., 2010; Di, Gohel, Kim, & Biswal, 2013; Fox et al., 2005; Yeo et al., 2011). Indeed, decomposing the whole brain into its fundamental gradients have revealed a structure for the organization of large scale networks, with the primary gradient trending from unimodal networks to multimodal networks (Margulies et al., 2016).

However, despite the overwhelming focus on large scale brain organization, detailing the particular patterns of connectivity from one region to another remains a challenge.

Region-to-region topographic connectivity has been observed between early visual areas, which show retinotopic organization (Dumoulin & Wandell, 2008; Wang, Mruczek, Arcaro, & Kastner, 2015). By systematically seeding functional connectivity from known functional gradients, it's been found that functional connectivity within a visual region, and between visual regions seem to follow along known eccentricity organization, along the anterior-posterior axis (Arcaro, Honey, Mruczek, Kastner, & Hasson, 2015). In other words, certain parts of a visual region that represent certain eccentricities are more likely to connect to the specific parts of other visual regions that represent similar eccentricities. While this type of systematic seeding is possible in areas with a known and measurable sensory topology, a more general model, such as connective field mapping (Haak et al., 2013), is useful for studying the connection topology of higher order regions. The previous connective field mapping technique fits 2 dimensional surface based population receptive fields (pRFs) using cortical signal from one region as the input to another region (Haak et al., 2013). This method has been used to model early visual areas, and demonstrate maintenance of retinotopic organization across these visual regions (Gravel et al., 2014; Haak et al., 2013).

It is unclear whether the linear pattern of connectivity observed in early visual cortex is dependent on a shared sensory topological organization, or whether it is present in any highly connected network. In particular, for multimodal regions such as the prefrontal cortex, while it is known that various subdivisions are closely connected, the exact functional organization remains controversial (Badre & Nee, 2018; Goldman-Rakic, 1999; Petrides, 2005; Ungerleider, Courtney, & Haxby, 1998). In theoretical models, spatial linearity in connectivity is postulated to serve the function of ensuring the fidelity of information transfer across a network (Thivierge & Marcus, 2007). Linear organization of connectivity also has the potential to generate complex abstract representations by

virtue of topographic overlap (Tinsley, 2009). This suggests that abstract computations can be performed by biases in spatial connectivity and filtering between regions of a large scale network, in the same way that has been suggested in the visual system (Tinsley, 2009; Van Essen & Gallant, 1994).

In this study, we have modified and extended the connective field model, allowing for the estimation of linearity of functional connectivity between regions using resting-state fMRI data in order to infer potential fidelity of information transfer between regions within and across unimodal and multimodal networks. This method fits a 3-D isotropic Gaussian to the connectivity pattern in the mapping region from individual voxels in the seed region (Fig. 1A). This fitting procedure produced four parameters, 3 location parameters describing the preferred locus of connectivity and a spread parameter, and the fitted Gaussian acts like an encoding model for timecourses of BOLD activity (Fig. 1B). We further estimated the degree of linear mapping from one region to another by performing Procrustes analysis. The degree to which these coordinates can be fit using a linear transformation provides the estimation of the linear mapping between them. We first examined the degree of linearity in the visual system, as the literature is relatively established, and then examined whether it is simply a specific case of a general motif of brain connectivity across various networks, and finally used this approach to test the two main theories of prefrontal functional organization.

2. Results

2.1 Mapping Dorsal Visual Cortex connectivity in Ventral Visual Cortex

We first used 3-D connective field modeling to show that dorsal and ventral portions of the visual cortex have a linear organization in their functional connectivity. Figure 2A illustrates the group 3-D connective field maps in the ventral visual cortex for two selected seed voxels in the dorsal visual cortex using the Cambridge Buckner dataset. An animation of all seed voxels and their corresponding modeled Gaussian maps is available in the supplemental materials. Fig. 2B summarizes these results as a vector field in the seed region, with a vector originated from each seed voxel displaying the location

of its preferred connectivity as the relative displacement from the center of the mapping region (Fig. 2B). This vector field of the dorsal visual cortex showed a strong connectivity mapping to the ventral visual cortex along the predicted anterior-posterior organization (Arcaro et al., 2015), which was also supported quantitatively by the high correlation between the seed's y-location and the mean modeled y-location of the Gaussian fit in the mapping region, with $r(394) = 0.71$, $p = 1.63 \times 10^{-62}$ ($r = 0.83$, with outliers removed). The spread or standard deviation parameter of the Gaussian model also increased along the seed region's y-axis (Fig. 2C left), which was supported quantitatively by the correlation between the seed's y-location and the modeled standard deviation parameter, with $r(394) = 0.61$, $p = 5.45 \times 10^{-42}$ (Fig 2C right). This relationship was similarly evident between the dorsal and ventral portions of V1, V1, and V3, using a set of more restricted masks (Fig. 3). The Procrustes analysis yields an estimation of 42.36% linear organization for the highly inclusive masks of dorsal and ventral occipital cortex that spans multiple sub regions, while the linearity estimates were substantially higher for the restrictively masked V1, V2, and V3: 68.79%, 67.45%, and 66.98%, respectively. These results together suggested that the inter-regional connectivity in early visual areas mirror the organization of eccentricity representation, with region to region connectivity ordered spatially along similar eccentricity locations, and the spread of that connectivity potentially following the increase in receptive field sizes toward more anterior visual cortex.

To evaluate the validity of our model, we examined the distribution of correlations between our predicted timecourses from the model and the actual BOLD timecourses (see Fig. 1B) for each voxel in the large dorsal visual cortex mask (Fig. S1, left). The distribution of r-values across all subjects and all their correspond timecourses when using the matching prediction is strictly positive, with a mean of 0.55. While the distribution of correlations produced by nonmatched pairs is much wider with a mean of close to zero (Fig. S1, right).

We also evaluated the stability of the 3-D connective field model within individual subjects and across mean results for the dorsal and ventral visual cortex, using the IBATRT dataset. For each subject, the estimated y-location parameters from the first and second runs were correlated across voxels (Fig. S2A). The resulting distribution of r-values had a median of 0.60, demonstrating moderate to good reliability at the individual subject level. At the group level, the mean parameters for each run correlated across voxels strongly, r = 0.98 (Fig. S2B).

Using the Midnight Scan Club (MSC) data, we showed that the median test-retest reliability within subjects increases with more scan time per subject, with the 150 minutes in each split leading to a test-retest reliability of 0.81 (Fig. S2C). A vector field of dorsal-ventral connectivity mapping for the visual cortex was generated for each individual (300 minutes of data from all sessions), and the anterior-posterior relationship was observed in every subject (Fig. S3). Quantitatively, the correlation between y-location modeled Gaussian parameter and seed y-location was high: ranging form 0.5 to 0.72 across the 10 individuals. In addition, linearity estimates for the entire dorsal and ventral visual cortex for each MSC individual ranged between 28.81%-51.45%, which is around the group estimates calculated from the Cambridge-Buckner data described above, albeit slightly lower. Similarly, linearity estimates of V1d→V1v were highly replicated in each MSC subject, ranging from 54.50% to 70.37%.

2.2 FFA connectivity bias

Higher order visual regions have been characterized as complex filters of early visual region information (Van Essen & Gallant, 1994), with this type of model shown to predict FFA activation during a task (Kay & Yeatman, 2017). Here, we examined to what extent the region to region connectivity reflect this filtering process. Using the Cambridge Buckner data, we applied the 3-D connective field mapping method to model the pattern of right FFA connectivity with V1 and compared its connectivity profile with that of PPA, a region which is selective to stimuli that have more peripherally distinctive features. In comparison to the PPA, the FFA showed more connectivity with

posterior V1, the part with more foveal receptive fields. This was evident both across subjects (Fig. 4A, left), $t(197) = -4.92$, $p = 1.86 \times 10^{-6}$, and across voxels (Fig. 4A, center), $t(226) = -3.85$, $p = 1.55 \times 10^{-4}$. In order to put the FFA's spatial pattern of connectivity with V1 in context with the prior results, we plotted the distribution of FFA-V1 connectivity against the dorsal visual cortex's distribution of connectivity with ventral visual cortex along the y-axis (Fig. 4A, right, and Fig. 4B). These results showed the more posteriorly oriented and convergent nature of the FFA's connectivity with V1. Indeed, the linearity estimate of V1→ FFA was substantially lower (7.23%) relative to connectivity among early visual regions (42.36%), whereas the Convergence Factor, a parameter derived from the ratio of pooled variance of the space of the region to the pooled variance of the fitted Gaussian parameters, was much larger for the V1→FFA (139.95) in comparison to early visual regions (8.48).

When an ideal model of V1 pRF organization was fed through the fitted model of connectivity between V1 and FFA, the FFA's pRF demonstrates a few classic hallmarks: a high degree of foveal representation, a larger receptive field, and even a slight bias towards the lower hemifield as seen in prior studies (Gomez, Natu, Jeska, Barnett, & Grill-Spector, 2018; Kay, Weiner, & Grill-Spector, 2015) (Fig. 4C & 4D). While only nine of the voxels in the V1 model overlap with the central location of the pRFs in the FFA, comparing voxels in the FFA directly to voxels in V1 sharing the same eccentricity and angle showed on average a larger receptive field in the FFA, $t(154) = 11.15$, $p = 4.92 \times 10^{-21}$ (Fig. 4E). This suggests an integration across voxels of different pRF locations, rather than a simple selective connectivity with centrally located pRFs in V1.

2.3 Linearity of connectivity organization across the whole brain

While the early visual system demonstrated high linearity in connectivity between regions, a fundamental question left unanswered is whether this is a special property of the early visual cortex or it is a general motif of cortico-cortical functional connectivity. To address this issue, we calculated the linearity of connectivity between all unique pairs of the 200 right hemisphere parcels in the Schaefer

parcellation. We used the MSC dataset for this analysis to ensure stable parameter estimates, given the long scan time. For each subject of the MSC dataset, the distribution of linearity across the brain was shifted significantly to the right relative to the permutation null distribution (Fig. 5A). The percentage of pairs for each subject that surpass the permutation $\alpha = .05$ ranges from 70.44 to 78.86% with the exception of two subjects of lower values. Note that one of the outliers, MSC08 (with linearity at 44.36%), was identified by the original investigators to have a significant proportion of time in a drowsy state, affecting this individual's BOLD data (Gordon et al., 2017).

Figure 5 illustrates the linear organization for three selected seed regions' connectivity with other regions across the entire right hemisphere (Fig. 5B). The flatmaps show a clear segregation of linearity values within and across the different networks, exemplified by seeding from anterior and posterior visual cortex demonstrating stronger linearity with different visual areas, middle frontal gyrus demonstrating stronger linearity with lateral prefrontal regions, and lower linearity between regions from different networks.

Further, nonmetric multidimensional scaling was applied to produce two dimensions that maximally reproduce the nonlinearity matrix (as a distance matrix) of the same 200 parcels (Fig. S5A, Fig. 6). The resulting primary mode was similar to large scale whole brain decompositions observed in previous studies of normal functional connectivity and genetic expression data (Margulies et al., 2016; Murray, Demirtaş, & Anticevic, 2018). This mode described a segregation lower order unimodal regions and higher order multimodal regions, with the negative end exemplified by visual and somatomotor networks and the positive end exemplified by default mode network. The second mode seemed to be a fractionation of the primary mode, potentially representing communication of information across these lower order/higher order boundaries.

2.4 Connectivity Organization of the Lateral Prefrontal Cortex

After illustrating the ubiquity of linear organization of functional connectivity across visual cortex and large networks, we specifically examined how gradients of linearity express in a highly multimodal structure such as the lateral prefrontal cortex. We found two gradients (Fig. S5B). Gradient 1 demonstrates an axis that segregates posterior middle frontal gyrus/inferior precentral sulcus and anterior inferior frontal gyrus/frontal pole (Fig. 7A Top Left). Gradient 2 demonstrates a diagonal axis, segregating posterior superior frontal gyrus and anterior inferior frontal gyrus (Fig. 7A Top Right). These two linearity gradients closely resemble the two prominent frameworks described in the literature to simplify the overall functional organization of the frontal cortex. One is often referred to as the domain specialization framework, suggesting that the dorsal and ventral lateral prefrontal cortices are preferentially organized to process spatial and nonspatial (e.g. objects) information, respectively, due to their differential connectivity with the dorsal and ventral visual streams (Goldman-Rakic, 1987). The second is an increase in abstraction along the rostral-caudal axis, with the more rostral regions linked to more abstract facets of behavioral control (e.g. Sensory perception → Context → Rule) (Koechlin, Ody, & Kouneiher, 2003). In addition, we performed nonmentric MDS on the standard voxelwise resting-state functional connectivity of the lateral prefrontal cortex, and found two gradient decompositions that mainly segregate middle frontal gyrus and inferior frontal gyrus from the rest of the frontal cortex (Fig. 7A, bottom).

To examine the extent that either of the theoretical frameworks for prefrontal organization were driving the uncovered linearity gradients in the prefrontal cortex, we constructed a linear regression for each gradient. More specifically, we tested whether the gradient organization can be predicted from the differential linear input from dorsal and ventral stream sources, superior parietal and anterior temporal, cortices, respectively (domain specialization framework) and/or from the average convergence factor of each frontal region with all other frontal regions (abstraction framework), while controlling for the mean linearity with all other frontal regions. The results are summarized in Table 1 (Fig. 7B for first

order correlations). We found that the first gradient was driven by both dorsal-ventral input and the convergence factor, though more strongly by the dorsal-ventral input ($\beta = -0.53$, $p < .01$; $\beta = 0.39$, $p < .05$). The second gradient, however, only had a detectable relationship with the convergence factor ($\beta = -0.42$, $p < .05$). In sum, while both gradients were, to some degree, related to these organizational features, Gradient 1 was most strongly related to differential dorsal-ventral input while Gradient 2 was most strongly related to mean convergence.

To put the gradient results in the context of the existing literature, we examined the mean gradient values of parcels derived from various topic based meta-analyses from Neurosynth that represent each of two prefrontal functional organizations. We found that indeed, Gradient 1 segregated spatial and object representation topics, and that Gradient 2 segregated motor response and higher order response control (response conflict) (Fig. 7C left). Importantly, the vectors determining these segregations are relatively orthogonal. In contrast, gradient maps of the voxelwise resting state functional connectivity demonstrates neither a clean segregation of these terms, nor the orthogonality of them (Fig. 7C right).

3. Discussion

Using a 3-D Gaussian modeling approach with whole-brain resting-state fMRI data, we found that closely connected cortical regions exhibit a relatively strong linear topology of their functional connectivity. This linear organization of region-to-region functional connectivity was highly reliable in early visual regions, following a topographic order along the anterior-posterior axis for eccentricity representation, as predicted by the literature (Arcaro et al., 2015; Gravel et al., 2014; Haak et al., 2013). In a higher order visual area, the FFA, the estimated connectivity profile seemed to reflect complex filtering of information, such that FFA connectivity to V1 produced the hypothesized patterns of bias towards the part of V1 that has more foveal representations, and this connectivity bias was sufficient to reproduce the main features of FFA's pRF. In the whole brain, linearity again emerged as a primary

topographic organization for functional connectivity among regions within large-scale networks, including the default mode and frontoparietal networks, while linearity was weaker between regions across different networks. Lastly, we found that the linearity and convergence patterns of connectivity in the lateral prefrontal cortex supports the two prevailing frameworks of prefrontal cortex functional organization, domain specialization and abstraction. Our overall findings thus suggest a ubiquitous nature of linearity in spatial organization of functional connectivity among closely related functional regions in the human brain.

3.1 Eccentricity dependent functional connectivity in early visual cortex as a special case of linear communication

We found that the early visual cortex demonstrates orderly region-to-region functional connectivity that maintains the organization of eccentricity representation across regions. This result replicates previous work that used resting state fMRI data and phase-locking fMRI task data in studies of retinotopic organization of the visual system (Arcaro et al., 2015; Gravel et al., 2014; Haak et al., 2013). The orderly functional connectivity likely contributes to the maintenance of retinotopic organization across the posterior cortical regions for multiple levels of visual processing. We also demonstrated that this motif breaks down for connectivity between early and higher order visual cortices (Fig. 4). The pattern of FFA connectivity, its convergence and selection of foveal resources, predicts some fundamental aspects of the receptive field properties of this structure, which is specialized for face processing (Kanwisher, McDermott, & Chun, 1997). These findings on region-to-region connectivity patterns provide a potential structure for understanding what information is maintained across regions, which would be useful for future modeling of information transformation and transfer from one region to another region (Basti et al., 2018; Thivierge & Marcus, 2007).

The linearity of connectivity observed in the early visual cortices seems to be a special case of a larger phenomenon. Our findings suggest that such a spatial layout of functional connectivity is a

probable general mode of communication across the brain (Fig. 5, 6), likely at least partially for the purposes of high fidelity information transmission across regions within a functional network (Thivierge & Marcus, 2007). In the visual cortex, coincidental activity that drives plasticity provides a potential mechanism for the generation and maintenance a spatially linear organization of communication between nearby regions (Catalano, Chang, & Shatz, 1997; Elliott & Shadbolt, 1996; Schoen, Leutenecker, Kreutzberg, & Singer, 1990). However, activity dependent synaptic pruning is not the only mechanism that drives organization in early visual cortex. Recent studies have suggested a form of proto-organization driven by genetic expression and their products (e.g. morphogens) in animal models of development and in humans (Arcaro & Livingstone, 2017; Cheng, Nakamoto, Bergemann, & Flanagan, 1995; Crowley & Katz, 2000). This mechanism of organization developing from molecular gradients is more widely observed, pertaining to many brain systems. For example, molecular signaling has been shown to be responsible for organization of thalamocortical connections in and ordered spatial gradient, with Emx2 and Pax2 regulating the anterior-posterior organization of cortical fields and their thalamic afferents (Bishop, Goudreau, & O'Leary, 2000). Using 3-D connective field modeling, we found a strong linear organization in lateral prefrontal areas despite a lack of clear or consistent retinotopy in these areas (Hagler & Sereno, 2006; Kastner et al., 2007). Strong linearity in the absence of retinotopy suggests a potential link with proto-organization. Indeed, our gradient decomposition of linearity resembles gradients of genetic expression (Burt et al., 2018; Murray et al., 2018) providing potential convergent evidence for this interpretation.

3.2 Linearity and computation within and across large-scale brain networks

Spatially linear organization of input-output relationships is thought to maintain information across levels of processing, allowing for precise action on continuous sensory information (Thivierge & Marcus, 2007). Topographic organization and projections from topographic space has been postulated to produce ordered abstract space as shown in connectionist models (Tinsley, 2009). With a continuous

space of abstract relations, complex information transformation in abstract space can be achieved by the same general mechanism as filtering of visual information. For example, this is the proposed mechanism underlying saliency map models, where information from many independent channels are combined topographically to represent the overall visual salience of an image (Itti & Koch, 2000; Roggeman, Fias, & Verguts, 2010). These saliency map models have been successful in predicting eye movements to complex visual stimuli, attentional load responses in parietal cortex, and even working memory capacity (Foulsham & Underwood, 2008; Knops, Piazza, Sengupta, Eger, & Melcher, 2014).

With the simple assumption information is spatially segregated, a tractable form of general computation in the brain is through spatial biases in connectivity, which would subsume the above description of linearity. Spatial biases can, however, have vastly different scopes. With distinct information converging onto a neuron giving rise to many potential combinations of that information, it has been shown that the exact combination is at least partially determined by spatial biases in convergence along the dendritic compartment (London & Häusser, 2005; Taylor, He, Levick, & Vaney, 2000). Higher order spatial biases, from cortical column to cortical column, may be responsible for higher order computation. Previous work has examined information transformation more directly, estimating linear transformations that map the representational dissimilarity matrices from one region to another (Basti et al., 2018). Our 3-D connective field model provides an appropriate description of the proposed mechanisms for these transformations, allowing for critical tests of this theory in observational data.

3.3 Organization of the Lateral Prefrontal Cortex Using Spatial Connectivity Metrics

Gradient decomposition of linearity of the prefrontal functional connectivity demonstrated evidence for two gradients of functional organization. Both prefrontal gradients (particularly Gradient 1) seem to be at least partially related to differential linear input from dorsal and ventral visual pathways. Previous studies have consistently found differential projections from dorsal and ventral

visual stream nodes to dorsal and ventral prefrontal cortex, respectively (Cavada & Goldman-Rakic, 1989; Goldman-Rakic, 1987; Kawamura & Naito, 1984). This segregation of dorsal and ventral pathway input into the prefrontal cortex has been supported both structurally and functionally in humans (Takahashi, Ohki, & Kim, 2013). This dorsal-ventral segregation of the prefrontal cortex has been shown to be differentially responsible for spatial and object working memory (Constantinidis & Qi, 2018). Indeed, inactivation of dorsal prefrontal cortex impairs spatial working memory, but not object working memory (Chafee & Goldman-Rakic, 2000; Clark, Noudoost, & Moore, 2014; Suzuki & Gottlieb, 2013). Thus, the differential input from dorsal and ventral streams has functional consequences, leading to the segregation of downstream dependence of higher order functions depending on the type of information being operated on.

While a prominent perspective of prefrontal organization, the domain specialization hypothesis of lateral prefrontal functional organization is not the only studied organizational principle. Accumulating evidence shows another prominent gradient of prefrontal functional organization along the anterior-posterior axis related to the level of abstraction, from the posterior representation of sensorimotor response selection to the more abstract representation of task goals/rules in the anterior portions of the prefrontal cortex (Azuar et al., 2014; Koechlin et al., 2003; Kouneiher, Charron, & Koechlin, 2009). By varying the rules and contexts of various tasks, it was found that areas related to the stimulus response mapping were located more caudally, while areas related to contexts and rules were more rostral (Azuar et al., 2014; Badre & D'Esposito, 2007; Koechlin et al., 2003). The gradients of linearity (particularly Gradient 2) seem to correspond well to this caudal to rostral representation of abstraction as well, as shown by the average convergence factor of each node (with each other node of the lateral prefrontal cortex).

In sum, on the basis of these new metrics of the spatial profile of functional connectivity, our data support both frameworks of functional organization for the lateral prefrontal cortex. Our results

support the existence of two orthogonal large scale organizational principles of the prefrontal cortex, bridging the two literatures, rather than putting them at odds. This is consistent with the previous literature examining functional connectivity which has found evidence for both dorsal-ventral and rostral-caudal organizations in the lateral prefrontal cortex (Blumenfeld, Nomura, Gratton, & D'Esposito, 2013; Schumacher, Schumacher, Schelter, & Kaller, 2019).

3.4 Limitations and future directions

Our estimations of linearity of connectivity between across regions were likely subjected to parcel selection, which is a limitation for this type of analysis. Given the multitude of parcellations and the multitude of methods used to obtain parcellations, the results could look slightly different if other justified parcellations were used. It is likely that our estimations of linearity would be even stronger with "true" parcels, given that more specification in early visual cortex actually boosted the estimated linearity (from ~42% to ~68%). In addition, the 3-D Gaussian model itself also has limitations and makes certain assumptions. For one, it assumes a single focal point of connectivity from one region to another, which is probably overly simplified. However, the final R^2 of the optimization procedure provides a marker for the fit of the model to the data; if these values are too low in the analysis, it would be inappropriate to make any conclusions about the fitted values. As the R^2 of the model tended to increase with more scan time, a large proportion of the misfit is likely due to noise. With the 30 minute sessions of the MSC data, the modal R^2 tended around 0.30-0.60, indicating a reasonable fit. Gaussian mixture models can be developed in the future to account some conditions of misfit, such as regions with multiple maxima.

It is important to note that the 3-D connective field method has a high dependence on high signal-to-noise ratio in single voxels, as opposed to the more conventional analyses that either use signal averaging within ROIs or smoothing to increase the signal-to-noise ratio. Because of this, higher resolution datasets may suffer from less stability due to the increase of proportion of thermal noise in

each voxel (Edelstein, Glover, Hardy, & Redington, 1986), though the impact on signal-to-noise ratio can potentially be counterbalanced by a reduction in physiological noise (Bodurka, Ye, Petridou, Murphy, & Bandettini, 2007). Further studies are needed to test our approach on higher resolution data. Optimally, the goal is to achieve a reliable connective field mapping at the size of functional columns of the regions of interest, which may be feasible in the frontal cortex, where columns may be as large as 800-900 micron (Hirata & Sawaguchi, 2008; Masse, Hodnefield, & Freedman, 2017).

3.5 Conclusions

By applying 3-D connective field modeling on resting-state fMRI data, we demonstrated that linearity of functional connectivity is likely common mode of communication across the cerebral cortex. This pattern of connectivity organization is most evident within the same functional network module, with the whole brain illustrating a primary gradient of linearity of functional connectivity comparable to two different data sources: resting-state functional connectivity and genetic expression. By the same principles, the functional connectivity of the lateral prefrontal cortex seemed to be organized around two axes: posterior middle frontal gyrus → anterior inferior frontal gyrus / frontopolar cortex (primarily spatial → object) and posterior superior frontal gyrus → anterior inferior frontal gyrus (primarily motor → response control). These findings show that deriving finer scale (voxel level) spatial organization of region to region connectivity in volumetric space seems to be useful in resting-state fMRI data. Vector field representations of region to region connectivity has the potential to be an informative visualization for information transfer and transformation from one region to another, with linearity and convergence factor as the quantitative metrics, especially if the voxel size can be reduced to the size of a cortical column in the regions of interest.

4. Materials and Methods

4.1 Subjects

We used three publicly available datasets: one sample of healthy controls with well validated resting state fMRI data, which is the Cambridge Buckner subset of the 1000 functional connectomes project (Biswal et al., 2010), and two smaller samples more well suited for test-retest reliability studies. The first small sample being the Intrinsic Brain Activity Test Retest (IBATRT) dataset (Zuo et al., 2014), and the second being the Midnight Scan Club (MSC) dataset (Gordon et al., 2017).

For the Cambridge Buckner data sample there were a total of 198 subjects (123 female), ages 18-30 (M = 21.03, SD = 2.31), with all subjects included in the final analysis. For the IBATRT data sample, there were a total of 36 subjects (18 female) ages 19-48 (M = 27.33, SD = 7.86) with two sessions and each with two runs. Four IBATRT subjects were excluded due to excessive motion in at least one of the four runs, leaving 32 subjects with data in the two runs of Session 1 (16 female; ages 19-48, M = 26.03, SD = 7.24). For the MSC dataset, there were a total of 10 subjects (5 female), ages 24-34 (M = 29.1, SD = 3.3), and all included in the final analysis.

4.2 fMRI Parameters

Cambridge Buckner data (Siemens 3T Trim Trio): T1-weighted images were collected with MPRAGE with the following image parameters: slices = 192, matrix size = 144 x 192, voxel resolution = 1.20 x 1.00 x 1.33 mm^3. Resting state fMRI data were T2*-weighted images acquired using EPI with the following parameters: 47 interleaved axial slices, TR = 3000 ms, voxel resolution = 3.0 x 3.0 x 3.0 mm^3 (119 volumes).

IBATRT data (Siemens 3T Trim Trio): T1 weighted images were collected with MPRAGE with the following image parameters: slices = 176, matrix size = 256 x 256, voxel resolution = 1.0 x 1.0 x 1.0 mm^3. Resting state fMRI data were T2*-weighted images acquired using EPI with the following parameters: 29 ascending axial slices, slice gap = 0.36 mm, TR = 1750 ms, voxel resolution = 3.4 x 3.4 x 3.6 mm^3 (343 volumes each run). While there were up to 4 runs across 2 sessions for subjects, we only utilized the two runs in the first session.

MSC Data (Siemens 3T Trim Trio): Four T1 weighted images were collected: slices = 224, voxel resolution = 0.8 x 0.8 x 0.8 mm^3. Four T2 weighted images: 224 slices, voxel resolution 0.8 x0.8 x 0.8 mm^3. Resting state fMRI were T2* weighted images acquired using EPI: 36 interleaved axial slices, TR = 2200 ms, voxel resolution = 4 x 4 x 4 mm^3 (818 volumes each session). A gradient echo field map was collected with the same parameters as the BOLD EPI images for each session. There were 10 sessions for each subject, all utilized in the analysis.

4.3 Image Preprocessing

For each individual in the Cambridge Buckner and IBATRT data samples, preprocessing was performed utilizing SPM12 (http://www.fil.ion.ucl.ac.uk/spm/software/spm12/). The functional images were first corrected for slice timing, and then realigned to the middle volume according to a 6 parameter rigid body transformation. Structural images were coregistered with the mean functional image, segmented, and then normalized to the MNI template using both linear and nonlinear transformations. Functional images were normalized utilizing the same parameters as the structural normalization.

Further preprocessing was performed following the standard procedures of resting-state fMRI analysis either using CONN (Whitfield-Gabrieli & Nieto-Castanon, 2012) or custom Matlab scripts. A nuisance regression was constructed with the following confounding variables: 6 motion parameters up to their second derivatives, scans with evidence of excessive motion (Framewise Displacement [FD] > .5 or DVARS > 5), session onset, estimated physiological signal generated through aCompCor (a temporal PCA of the white matter and CSF voxels with the number of components included determined individually on the basis of a Monte Carlo null model (Behzadi, Restom, Liau, & Liu, 2007)), and a linear drift component. For the Cambridge Buckner data the residuals from the nuisance regression were filtered utilizing a bandpass between the frequencies of 0.008 and 0.09 Hz, while for the IBATRT

data, the band-pass filtering and nuisance regression were done simultaneously (Hallquist, Hwang, & Luna, 2013). Finally, the resultant data were despiked using a tangent squashing function.

For the MSC data, we utilized their release of preprocessed data which includes slice intensity correction, mode 1000 intensity normalization, realignment, transformation into Talairach space and FSL's field distortion correction (Smith et al., 2004). These data also came with additional preprocessing for resting-state analysis. Censored volumes were determined by an FD threshold of 0.2 mm. The data were first demeaned and detrended, then a nuisance regression was performed removing the following factors, with censored volumes ignored: global signal, white matter mean signal, CSF mean signal, and motion regressors with the full Volterra expansion. The data were then interpolated across the censored volumes using least squares spectral estimation followed by band-pass filtering between 0.009 and 0.08 Hz. The censored volumes were removed in the final resultant data samples for analysis (see Gordon et al., 2017 for full description of processing pipeline).

4.4 Regions of Interest

The initial analyses of 3-D connective field mapping were conducted using the visual areas as regions of interest (ROIs). For the early visual areas, we utilized the probabilistic visual atlas (Wang et al., 2015), selecting all voxels with any probability of either dorsal or ventral visual cortex, with no overlap between the two ROIs (see Fig. 2A). To determine whether the finding from the overall visual cortex mask was a general property of early visual areas, we also defined more selective masks of the dorsal and ventral portions of V1, V2, and V3, each with probability greater than 30% to reduce overlap between the masks. We then applied the same connective field mapping analyses across each visual region's dorsal and ventral portions.

In an additional analysis, we created slightly more lenient V1 mask selecting any voxels that have a greater than 15% probability of being V1. We used this V1 ROI as a mapping region for the right fusiform face area (FFA) and the right parahippocampal place area (PPA), both FFA and PPA were

derived using Neurosynth meta-analyses, with “faces” and “place” as keywords, respectively (Yarkoni, Poldrack, Nichols, Van Essen, & Wager, 2011).

For the whole brain linearity of connectivity analysis, we made use of a previously published whole brain parcellation atlas of 400 regions. The parcels were generated by maximizing correlations within a parcel while minimizing local changes in correlations within a parcel (Schaefer et al., 2018). For time and computational feasibility, we only used the 200 parcels of the right hemisphere.

4.5 3-D Connective field mapping and model parameters

For both the “seed” and “mapping” regions, the mean timecourse of the ROI was subtracted from each voxel’s timecourse, so as to reduce the influence of correlation at the mean signal level, though in practice the results are similar with or without removing the means. Then, for each voxel within the “seed” region, we calculated its correlation with every voxel within the “mapping” region and transformed the resulting correlation values using Fisher’s Z transformation. Each distribution of Fisher’s Z values (for each seed voxel) was fitted with a 3-D isotropic Gaussian distribution (Fig. 1A):

$$g_v(x,y,z)=\frac{1}{\sigma^3(2\pi)^{3/2}}\exp-\frac{(x-x_0)^2+(y-y_0)^2+(z-z_0)^2}{2\sigma^2}$$

Initial values for the x_0, y_0, and z_0 parameters during the optimization procedure were the x, y, and z locations of the maximum Fisher’s Z value, and an arbitrarily small number (floating point epsilon) for the standard deviation. The optimization procedure had a lower bounds of the smallest location parameters within the mapping region and the floating point epsilon for the standard deviation, while the upper bounds were the maximum location parameters and the smallest range of the 3 dimensions for the standard deviation. The parameters of the Gaussian were estimated by minimizing the correlation distance between the Fisher’s Z values and the Gaussian probability density function using the interior-point algorithm (Byrd, Gilbert, & Nocedal, 2000), implemented by MATLAB’s fmincon function (MathWorks Inc, 1995-2019). Predicted time-series for each voxel v in the seed region were

estimated as the degree of overlap between the estimated Gaussian function and the activation pattern of the mapping region for each time-point t (Fig. 1B):

$$p_v(t)=\sum_x \sum_y \sum_z A(x,y,z,t)g_v(x,y,z)$$

Both the predicted time-series and the actual data time-series were z-scored to remove any arbitrary scaling factors. Fit was assessed by comparing the distribution of correlations between the each voxel's fitted model and the true data to the distribution of correlation between each voxel's true data and every other voxel's fitted model.

Linearity of the connectivity from one region to another was estimated by fitting 3 space parameters of the Gaussian model to the 3 space parameters of the seed locations using Procrustes analysis (Kendall, 1989). The complement of the dissimilarity of the fit between the final output and the actual seed locations can be used as a direct measure of the degree of linearity of the mapping from one region to another. To visualize this transformation, a vector field can be created, with each vector originating at each seed voxel, and the orientation and length of the vector determined by the centered space parameters, it's preferred location in the mapping region in relation to the center of mass of the mapping region.

We also calculated a metric of convergence as the ratio of the spatial variance of the mapping region with the spatial variance of the Gaussian parameters:

$$Convergence\ Factor=\frac{\sigma_x^2+\sigma_y^2+\sigma_z^2}{\sigma_{x_0}^2+\sigma_{y_0}^2+\sigma_{z_0}^2}$$

This metric approaches 1 when the spread of connectivity is similar in size to the potential space it can connect to, regardless as to whether the connectivity is ordered or not. This value is greater than 1 when the connectivity only reaches a sub-portion of the region, indicating convergence. This factor is likely inflated when calculating over group averaged data, as the average pulls values away from the

edges, but should be comparable in the relative sense regardless. The relationship between convergence factor and linearity is shown in Figure S4.

This 3-D connective field mapping analysis has been released in the form of a MATLAB toolbox, with a simple GUI wrapper to help guide analysis (www.nitrc.org/projects/r2r_prf/). This approach represents a simplification and extension of previous work.

We assessed test-retest reliability using the IBATRT and MSC datasets. For the IBATRT dataset, we examined the spatial correlation between the patterns of parameters in run 1 and run 2, within individual subjects and across session means. For the MSC dataset, we examined potential effects of added scan time to the stability of the 3-D Gaussian parameters for individual subjects. We split the each subjects' sessions into two groups, a test and a retest group. We varied the number of sessions in each group, with a maximum of 5 session per group, and calculated the test-retest reliability for each subject. We also performed 3-D connective field mapping for each subject with all their sessions to demonstrate the stability of the group effect at the level of individual subjects.

4.6 Deriving FFA pRF features from ideal V1 model

To study how the pRF features of the right FFA may be a result of biased connectivity from the earlier visual regions, we constructed an ideal model of pRFs in V1 on the basis of prior work in retinotopic mapping (Dumoulin & Wandell, 2008; Mackey, Winawer, & Curtis, 2017) with two orthogonal dimensions, one for eccentricity in the anterior-posterior dimension and one for angular representation in the dorsal-ventral dimension, with pRF size varying linearly in accordance to eccentricity. We then used the fitted 3-D connective field map from FFA (seed) to V1 (mapping) to produce a visual field response profile for each voxel within the FFA as a weighted mixture of the response profiles from the ideal V1 model. Then, we fit a 2-D Gaussian to each voxel's response profile to produce a pRF for each voxel within FFA.

4.7 Whole brain characterization of linearity of functional connectivity

We performed 3-D connective field mapping on each unique pair between all possible pairs out of the 200 parcels in the right hemisphere of the Shaefer atlas for each subject in the MSC data. For each fitted pair, we calculated the linearity of connectivity using Procrustes analysis. First, we tested whether or not the distribution of linearity across all pairs of parcels across the brain for each subject were different than a permuted null distribution. This test was to demonstrate how typical linear relationships of connectivity are across the whole brain, and whether they can be generalized as a typical motif of inter-regional connectivity. We further selected several regions to test whether linearity is maintained through specific networks or generally across the brain.

Lastly, to compare with previous whole brain gradient decompositions (Margulies et al., 2016; Murray et al., 2018), we performed multidimensional scaling on the linearity matrices from all parcel pairs to estimate the primary and secondary gradients across the right hemisphere. The far ends of these gradients were considered to represent which regions maintain linear information across the brain. We produced a 2 dimensional solution, on the basis of an elbow in the plot of the rank correlation of the produced distance and the observed distance matrices (Fig. S5), and visualized the gradients across the brain, demonstrating the potential top two modes of linear communication across the right hemisphere.

4.8 Lateral Prefrontal Cortex Analysis

We selected the subset of parcels (see Section 4.7) within the lateral prefrontal cortex, and performed a similar gradient decomposition analysis specifically on prefrontal functional connectivity linearity. We estimated two gradients (see Fig. S5 for rational) of the lateral prefrontal cortex and then examined whether the discovered organization reflects principles of prefrontal cortex organization described in the literature (Goldman-Rakic, 1987; Koechlin et al., 2003). We also examined the gradients resulting from voxelwise functional connectivity for comparison. We tested two dominant hypotheses of the organization of the prefrontal cortex, domain specialization and abstraction. For the

domain specialization hypothesis, we calculated the linearity from the superior parietal lobe and the anterior temporal lobe to all lateral prefrontal parcels. We then z-scored each of the linearity values for each region and then subtracted them from each other. This metric is our stand in for the domain specialization hypothesis. For the abstraction hypothesis, we calculated the convergence factor from each prefrontal parcel to each of the other prefrontal parcels, and calculated the average convergence factor for that parcel. We also calculated the average linearity of each prefrontal parcel to each of the other prefrontal parcels as a control for the convergence factor. We then performed two linear regressions, one for each gradient, to evaluate how consistent these organizational frameworks are with the gradient decomposition of linearity. Each regression contained the following variables: the domain specialization variable, the abstraction variable, and the average linearity from each parcel to each other parcel in the prefrontal cortex.

To further confirm the relationship between these two prefrontal gradients and the two theories of organization, we generated masks on the basis of 4 (of 400) latent Dirichlet analysis derived compositions of term based meta-analyses using Neurosynth (Poldrack et al., 2012; Yarkoni et al., 2011). We chose a composition that suggested a maintenance of spatial information (Topic 110: visual, areas, stimulus, primary, perceptual, input, hemifield, sensory, human, fixation, retinotopic, visually, order, central, experiments, concurrent, top, objects, vision, presentation, pathways, inputs, stage, visuospatial, unilateral, checkerboard, calcarine, stronger, modulated, earlier, efficient, dot, gratings, hemifields, depended, received, dissociated, localized, hv, guide), one that suggested object representation (Topic 71: knowledge, tool, tools, living, semantic, conceptual, representations, familiar, critical, pantomimes, viewed, objects, world, classes, stored, representing, graspable, typical, nonliving, mechanical, learned, equally, retrieving, class, determined, defined, postures, actual, storing, independent, apraxic, daily, respective, verification, lif, affordances, inappropriate, affordance, articulated, dlfpc), one that suggested direct stimulus driven motor responses (Topic 11: motor, finger,

movements, movement, tapping, sensorimotor, activation, index, primary, simple, paced, sequential, ipsilateral, fingers, healthy, handed, triggered, execution, hz, thumb, flexion, rate, dystonia, cued, opposition, repetitive, extension, initiated, externally, unilateral, visually, contribution, hands, sequence, initiation, volunteers, digit, focal, digits, studied), and finally one that suggested a higher order response selection (Topic 123: conflict, interference, stroop, task, control, incongruent, response, resolution, cognitive, trials, congruent, behavioral, simon, monitoring, flanker, irrelevant, stimulus, word, relevant, attentional, conflicting, performance, conflicts, adjustments, neutral, resolve, color, event, counting, situations, congruency, modified, types, competing, activated, resolving, detecting, mechanisms, detection, interfering). We then extracted the mean gradient values of our linearity decomposition maps and the resting state decomposition maps from these meta-analysis based masks, examining whether or not the different sides of the linearity gradients segregate the terms in the way we would predict on the basis of our regression analysis, that is that the first gradient should largely segregate the stimulus based activation, while the second gradient should largely segregate the response abstraction based activation.

5. Conflicts of Interest

The authors disclose that there are no conflicts of interest relating to this work.

References

Arcaro, M. J., Honey, C. J., Mruczek, R. E., Kastner, S., & Hasson, U. (2015). Widespread correlation patterns of fMRI signal across visual cortex reflect eccentricity organization. *ELife*, *4*, e03952. https://doi.org/10.7554/eLife.03952

Arcaro, M. J., & Livingstone, M. S. (2017). A hierarchical, retinotopic proto-organization of the primate visual system at birth. *ELife*, *6*, e26196. https://doi.org/10.7554/eLife.26196

Azuar, C., Reyes, P., Slachevsky, A., Volle, E., Kinkingnehun, S., Kouneiher, F., … Levy, R. (2014). Testing the model of caudo-rostral organization of cognitive control in the human with frontal lesions. *NeuroImage*, *84*, 1053–1060. https://doi.org/10.1016/j.neuroimage.2013.09.031

Badre, D., & D'Esposito, M. (2007). Functional Magnetic Resonance Imaging Evidence for a Hierarchical Organization of the Prefrontal Cortex. *Journal of Cognitive Neuroscience*, *19*(12), 2082–2099. https://doi.org/10.1162/jocn.2007.19.12.2082

Badre, D., & Nee, D. E. (2018). Frontal Cortex and the Hierarchical Control of Behavior. *Trends in Cognitive Sciences*, *22*(2), 170–188. https://doi.org/10.1016/j.tics.2017.11.005

Basti, A., Mur, M., Kriegeskorte, N., Pizzella, V., Marzetti, L., & Hauk, O. (2018). Analysing linear multivariate pattern transformations in neuroimaging data. *BioRxiv*, 497180. https://doi.org/10.1101/497180

Behzadi, Y., Restom, K., Liau, J., & Liu, T. T. (2007). A component based noise correction method (CompCor) for BOLD and perfusion based fMRI. *NeuroImage*, *37*(1), 90–101. https://doi.org/10.1016/j.neuroimage.2007.04.042

Bishop, K. M., Goudreau, G., & O'Leary, D. D. M. (2000). Regulation of Area Identity in the Mammalian Neocortex by Emx2 and Pax6. *Science*, *288*(5464), 344–349. https://doi.org/10.1126/science.288.5464.344

Biswal, B. B., Mennes, M., Zuo, X.-N., Gohel, S., Kelly, C., Smith, S. M., … Milham, M. P. (2010). Toward discovery science of human brain function. *Proceedings of the National Academy of Sciences*, *107*(10), 4734–4739. https://doi.org/10.1073/pnas.0911855107

Blumenfeld, R. S., Nomura, E. M., Gratton, C., & D'Esposito, M. (2013). Lateral Prefrontal Cortex is Organized into Parallel Dorsal and Ventral Streams Along the Rostro-Caudal Axis. *Cerebral Cortex*, *23*(10), 2457–2466. https://doi.org/10.1093/cercor/bhs223

Bodurka, J., Ye, F., Petridou, N., Murphy, K., & Bandettini, P. A. (2007). Mapping the MRI voxel volume in which thermal noise matches physiological noise—Implications for fMRI. *NeuroImage*, *34*(2), 542–549. https://doi.org/10.1016/j.neuroimage.2006.09.039

Burt, J. B., Demirtaş, M., Eckner, W. J., Navejar, N. M., Ji, J. L., Martin, W. J., … Murray, J. D. (2018). Hierarchy of transcriptomic specialization across human cortex captured by structural neuroimaging topography. *Nature Neuroscience*, *21*(9), 1251. https://doi.org/10.1038/s41593-018-0195-0

Byrd, R. H., Gilbert, J. C., & Nocedal, J. (2000). A trust region method based on interior point techniques for nonlinear programming. *Mathematical Programming*, *89*(1), 149–185. https://doi.org/10.1007/PL00011391

Catalano, S. M., Chang, C. K., & Shatz, C. J. (1997). Activity-Dependent Regulation of NMDAR1 Immunoreactivity in the Developing Visual Cortex. *Journal of Neuroscience*, *17*(21), 8376–8390. https://doi.org/10.1523/JNEUROSCI.17-21-08376.1997

Cavada, C., & Goldman-Rakic, P. S. (1989). Posterior parietal cortex in rhesus monkey: II. Evidence for segregated corticocortical networks linking sensory and limbic areas with the frontal lobe. *The Journal of Comparative Neurology*, *287*(4), 422–445. https://doi.org/10.1002/cne.902870403

Cavada, C., & Goldman-Rakic, P. S. (1991). Topographic segregation of corticostriatal projections from posterior parietal subdivisions in the macaque monkey. *Neuroscience*, *42*(3), 683–696. https://doi.org/10.1016/0306-4522(91)90037-O

Chafee, M. V., & Goldman-Rakic, P. S. (2000). Inactivation of Parietal and Prefrontal Cortex Reveals Interdependence of Neural Activity During Memory-Guided Saccades. *Journal of Neurophysiology*, *83*(3), 1550–1566. https://doi.org/10.1152/jn.2000.83.3.1550

Cheng, H.-J., Nakamoto, M., Bergemann, A. D., & Flanagan, J. G. (1995). Complementary gradients in expression and binding of ELF-1 and Mek4 in development of the topographic retinotectal projection map. *Cell*, *82*(3), 371–381. https://doi.org/10.1016/0092-8674(95)90426-3

Clark, K. L., Noudoost, B., & Moore, T. (2014). Persistent Spatial Information in the FEF during Object-based Short-term Memory Does Not Contribute to Task Performance. *Journal of Cognitive Neuroscience*, *26*(6), 1292–1299. https://doi.org/10.1162/jocn_a_00599

Constantinidis, C., & Qi, X.-L. (2018). Representation of Spatial and Feature Information in the Monkey Dorsal and Ventral Prefrontal Cortex. *Frontiers in Integrative Neuroscience*, *12*. https://doi.org/10.3389/fnint.2018.00031

Crowley, J. C., & Katz, L. C. (2000). Early development of ocular dominance columns. *Science (New York, N.Y.)*, *290*(5495), 1321–1324. https://doi.org/10.1126/science.290.5495.1321

Di, X., Gohel, S., Kim, E. H., & Biswal, B. B. (2013). Task vs. Rest—Different network configurations between the coactivation and the resting-state brain networks. *Frontiers in Human Neuroscience*, *7*. https://doi.org/10.3389/fnhum.2013.00493

Dumoulin, S. O., & Wandell, B. A. (2008). Population receptive field estimates in human visual cortex. *NeuroImage*, *39*(2), 647–660. https://doi.org/10.1016/j.neuroimage.2007.09.034

Edelstein, W. A., Glover, G. H., Hardy, C. J., & Redington, R. W. (1986). The intrinsic signal-to-noise ratio in NMR imaging. *Magnetic Resonance in Medicine*, *3*(4), 604–618. https://doi.org/10.1002/mrm.1910030413

Elliott, T., & Shadbolt, N. R. (1996). A mathematical model of activity–dependent, anatomical segregation induced by competition for neurotrophic support. *Biological Cybernetics*, *75*(6), 463–470. https://doi.org/10.1007/s004220050311

Foulsham, T., & Underwood, G. (2008). What can saliency models predict about eye movements? Spatial and sequential aspects of fixations during encoding and recognition. *Journal of Vision*, *8*(2), 6–6. https://doi.org/10.1167/8.2.6

Fox, M. D., Snyder, A. Z., Vincent, J. L., Corbetta, M., Essen, D. C. V., & Raichle, M. E. (2005). The human brain is intrinsically organized into dynamic, anticorrelated functional networks.

Proceedings of the National Academy of Sciences, *102*(27), 9673–9678. https://doi.org/10.1073/pnas.0504136102

Goldman-Rakic, P. (1987). *Handbook of Physiology: The Nervous System: Higher Functions of the Brain, Vol. 5, Sect. 1*.

Goldman-Rakic, P. S. (1999). The physiological approach: Functional architecture of working memory and disordered cognition in schizophrenia. *Biological Psychiatry*, *46*(5), 650–661. https://doi.org/10.1016/S0006-3223(99)00130-4

Gomez, J., Natu, V., Jeska, B., Barnett, M., & Grill-Spector, K. (2018). Development differentially sculpts receptive fields across early and high-level human visual cortex. *Nature Communications*, *9*(1). https://doi.org/10.1038/s41467-018-03166-3

Gordon, E. M., Laumann, T. O., Gilmore, A. W., Newbold, D. J., Greene, D. J., Berg, J. J., … Dosenbach, N. U. F. (2017). Precision Functional Mapping of Individual Human Brains. *Neuron*, *95*(4), 791-807.e7. https://doi.org/10.1016/j.neuron.2017.07.011

Gravel, N., Harvey, B., Nordhjem, B., Haak, K. V., Dumoulin, S. O., Renken, R., … Cornelissen, F. W. (2014). Cortical connective field estimates from resting state fMRI activity. *Frontiers in Neuroscience*, *8*. https://doi.org/10.3389/fnins.2014.00339

Haak, K. V., Winawer, J., Harvey, B. M., Renken, R., Dumoulin, S. O., Wandell, B. A., & Cornelissen, F. W. (2013). Connective field modeling. *NeuroImage*, *66*, 376–384. https://doi.org/10.1016/j.neuroimage.2012.10.037

Haber, S. N., Fudge, J. L., & McFarland, N. R. (2000). Striatonigrostriatal Pathways in Primates Form an Ascending Spiral from the Shell to the Dorsolateral Striatum. *Journal of Neuroscience*, *20*(6), 2369–2382.

Hagler, D. J., & Sereno, M. I. (2006). Spatial maps in frontal and prefrontal cortex. *NeuroImage*, *29*(2), 567–577. https://doi.org/10.1016/j.neuroimage.2005.08.058

Hallquist, M. N., Hwang, K., & Luna, B. (2013). The nuisance of nuisance regression: Spectral misspecification in a common approach to resting-state fMRI preprocessing reintroduces noise

and obscures functional connectivity. *NeuroImage*, *82*, 208–225. https://doi.org/10.1016/j.neuroimage.2013.05.116

Hirata, Y., & Sawaguchi, T. (2008). Functional columns in the primate prefrontal cortex revealed by optical imaging in vitro. *Neuroscience Research*, *61*(1), 1–10. https://doi.org/10.1016/j.neures.2008.01.003

Hoover, J. E., & Strick, P. L. (1993). Multiple output channels in the basal ganglia. *Science*, *259*(5096), 819–821. https://doi.org/10.1126/science.7679223

Hubel, D. H., & Wiesel, T. N. (1962). Receptive fields, binocular interaction and functional architecture in the cat's visual cortex. *The Journal of Physiology*, *160*(1), 106–154. https://doi.org/10.1113/jphysiol.1962.sp006837

Itti, L., & Koch, C. (2000). A saliency-based search mechanism for overt and covert shifts of visual attention. *Vision Research*, *40*(10), 1489–1506. https://doi.org/10.1016/S0042-6989(99)00163-7

Kanwisher, N., McDermott, J., & Chun, M. M. (1997). The fusiform face area: A module in human extrastriate cortex specialized for face perception. *The Journal of Neuroscience*, *17*(11), 4302–4311.

Kastner, S., DeSimone, K., Konen, C. S., Szczepanski, S. M., Weiner, K. S., & Schneider, K. A. (2007). Topographic Maps in Human Frontal Cortex Revealed in Memory-Guided Saccade and Spatial Working-Memory Tasks. *Journal of Neurophysiology*, *97*(5), 3494–3507. https://doi.org/10.1152/jn.00010.2007

Kawamura, K., & Naito, J. (1984). Corticocortical projections to the prefrontal cortex in the rhesus monkey investigated with horseradish peroxidase techniques. *Neuroscience Research*, *1*(2), 89–103. https://doi.org/10.1016/S0168-0102(84)80007-3

Kay, K. N., Weiner, K. S., & Grill-Spector, K. (2015). Attention Reduces Spatial Uncertainty in Human Ventral Temporal Cortex. *Current Biology*, *25*(5), 595–600. https://doi.org/10.1016/j.cub.2014.12.050

Kay, K. N., & Yeatman, J. D. (2017). Bottom-up and top-down computations in word-and face-selective cortex. *Elife*, *6*, e22341.

Kendall, D. G. (1989). A Survey of the Statistical Theory of Shape. *Statistical Science*, *4*(2), 87–99. https://doi.org/10.1214/ss/1177012582

Knops, A., Piazza, M., Sengupta, R., Eger, E., & Melcher, D. (2014). A Shared, Flexible Neural Map Architecture Reflects Capacity Limits in Both Visual Short-Term Memory and Enumeration. *Journal of Neuroscience*, *34*(30), 9857–9866. https://doi.org/10.1523/JNEUROSCI.2758-13.2014

Koechlin, E., Ody, C., & Kouneiher, F. (2003). The Architecture of Cognitive Control in the Human Prefrontal Cortex. *Science*, *302*(5648), 1181–1185. https://doi.org/10.1126/science.1088545

Kouneiher, F., Charron, S., & Koechlin, E. (2009). Motivation and cognitive control in the human prefrontal cortex. *Nature Neuroscience*, *12*(7), 939–945. https://doi.org/10.1038/nn.2321

Kravitz, D. J., Saleem, K. S., Baker, C. I., & Mishkin, M. (2011). A new neural framework for visuospatial processing. *Nature Reviews Neuroscience*, *12*(4), 217–230. https://doi.org/10.1038/nrn3008

Kravitz, D. J., Saleem, K. S., Baker, C. I., Ungerleider, L. G., & Mishkin, M. (2013). The ventral visual pathway: An expanded neural framework for the processing of object quality. *Trends in Cognitive Sciences*, *17*(1), 26–49. https://doi.org/10.1016/j.tics.2012.10.011

London, M., & Häusser, M. (2005). Dendritic Computation. *Annual Review of Neuroscience*, *28*(1), 503–532. https://doi.org/10.1146/annurev.neuro.28.061604.135703

Mackey, W. E., Winawer, J., & Curtis, C. E. (2017). Visual field map clusters in human frontoparietal cortex. *Elife*, *6*, e22974.

Margulies, D. S., Ghosh, S. S., Goulas, A., Falkiewicz, M., Huntenburg, J. M., Langs, G., … Smallwood, J. (2016). Situating the default-mode network along a principal gradient of macroscale cortical organization. *Proceedings of the National Academy of Sciences*, *113*(44), 12574–12579. https://doi.org/10.1073/pnas.1608282113

Masse, N. Y., Hodnefield, J. M., & Freedman, D. J. (2017). Mnemonic Encoding and Cortical Organization in Parietal and Prefrontal Cortices. *The Journal of Neuroscience*, *37*(25), 6098–6112. https://doi.org/10.1523/JNEUROSCI.3903-16.2017

Murray, J. D., Demirtaş, M., & Anticevic, A. (2018). Biophysical Modeling of Large-Scale Brain Dynamics and Applications for Computational Psychiatry. *Biological Psychiatry: Cognitive Neuroscience and Neuroimaging*, *3*(9), 777–787. https://doi.org/10.1016/j.bpsc.2018.07.004

Petrides, M. (2005). Lateral prefrontal cortex: Architectonic and functional organization. *Philosophical Transactions of the Royal Society B: Biological Sciences*, *360*(1456), 781–795. https://doi.org/10.1098/rstb.2005.1631

Poldrack, R. A., Mumford, J. A., Schonberg, T., Kalar, D., Barman, B., & Yarkoni, T. (2012). Discovering Relations Between Mind, Brain, and Mental Disorders Using Topic Mapping. *PLOS Computational Biology*, *8*(10), e1002707. https://doi.org/10.1371/journal.pcbi.1002707

Roggeman, C., Fias, W., & Verguts, T. (2010). Salience maps in parietal cortex: Imaging and computational modeling. *NeuroImage*, *52*(3), 1005–1014. https://doi.org/10.1016/j.neuroimage.2010.01.060

Schaefer, A., Kong, R., Gordon, E. M., Laumann, T. O., Zuo, X.-N., Holmes, A. J., … Yeo, B. T. T. (2018). Local-Global Parcellation of the Human Cerebral Cortex from Intrinsic Functional Connectivity MRI. *Cerebral Cortex*, *28*(9), 3095–3114. https://doi.org/10.1093/cercor/bhx179

Schoen, S. W., Leutenecker, B., Kreutzberg, G. W., & Singer, W. (1990). Ocular dominance plasticity and developmental changes of 5′-nucleotidase distributions in the kitten visual cortex. *Journal of Comparative Neurology*, *296*(3), 379–392. https://doi.org/10.1002/cne.902960304

Schumacher, F. K., Schumacher, L. V., Schelter, B. O., & Kaller, C. P. (2019). Functionally dissociating ventro-dorsal components within the rostro-caudal hierarchical organization of the human prefrontal cortex. *NeuroImage*, *185*, 398–407. https://doi.org/10.1016/j.neuroimage.2018.10.048

Smith, S. M., Jenkinson, M., Woolrich, M. W., Beckmann, C. F., Behrens, T. E. J., Johansen-Berg, H., … Matthews, P. M. (2004). Advances in functional and structural MR image analysis and implementation as FSL. *NeuroImage*, *23*, S208–S219. https://doi.org/10.1016/j.neuroimage.2004.07.051

Suzuki, M., & Gottlieb, J. (2013). Distinct neural mechanisms of distractor suppression in the frontal and parietal lobe. *Nature Neuroscience*, *16*(1), 98–104. https://doi.org/10.1038/nn.3282

Takahashi, E., Ohki, K., & Kim, D.-S. (2013). Dissociation and convergence of the dorsal and ventral visual working memory streams in the human prefrontal cortex. *NeuroImage*, *65*, 488–498. https://doi.org/10.1016/j.neuroimage.2012.10.002

Tanaka, K. (1997). Mechanisms of visual object recognition: Monkey and human studies. *Current Opinion in Neurobiology*, *7*(4), 523–529.

Taylor, W. R., He, S., Levick, W. R., & Vaney, D. I. (2000). Dendritic Computation of Direction Selectivity by Retinal Ganglion Cells. *Science*, *289*(5488), 2347–2350. https://doi.org/10.1126/science.289.5488.2347

Thivierge, J.-P., & Marcus, G. F. (2007). The topographic brain: From neural connectivity to cognition. *Trends in Neurosciences*, *30*(6), 251–259. https://doi.org/10.1016/j.tins.2007.04.004

Tinsley, C. J. (2009). Creating abstract topographic representations: Implications for coding, learning and reasoning. *Biosystems*, *96*(3), 251–258. https://doi.org/10.1016/j.biosystems.2009.03.003

Ungerleider, L. G., Courtney, S. M., & Haxby, J. V. (1998). A neural system for human visual working memory. *Proceedings of the National Academy of Sciences*, *95*(3), 883–890. https://doi.org/10.1073/pnas.95.3.883

Van Essen, D. C., & Gallant, J. L. (1994). Neural mechanisms of form and motion processing in the primate visual system. *Neuron*, *13*(1), 1–10.

Wang, L., Mruczek, R. E. B., Arcaro, M. J., & Kastner, S. (2015). Probabilistic Maps of Visual Topography in Human Cortex. *Cerebral Cortex*, *25*(10), 3911–3931. https://doi.org/10.1093/cercor/bhu277

Whitfield-Gabrieli, S., & Nieto-Castanon, A. (2012). Conn: A Functional Connectivity Toolbox for Correlated and Anticorrelated Brain Networks. *Brain Connectivity*, *2*(3), 125–141. https://doi.org/10.1089/brain.2012.0073

Wolpert, D. M., & Flanagan, J. R. (2001). Motor prediction. *Current Biology*, *11*(18), R729–R732. https://doi.org/10.1016/S0960-9822(01)00432-8

Yarkoni, T., Poldrack, R. A., Nichols, T. E., Van Essen, D. C., & Wager, T. D. (2011). Large-scale automated synthesis of human functional neuroimaging data. *Nature Methods*, *8*(8), 665–670. https://doi.org/10.1038/nmeth.1635

Yeo, B. T. T., Krienen, F. M., Sepulcre, J., Sabuncu, M. R., Lashkari, D., Hollinshead, M., … Buckner, R. L. (2011). The organization of the human cerebral cortex estimated by intrinsic functional connectivity. *Journal of Neurophysiology*, *106*(3), 1125–1165. https://doi.org/10.1152/jn.00338.2011

Zuo, X.-N., Anderson, J. S., Bellec, P., Birn, R. M., Biswal, B. B., Blautzik, J., … Milham, M. P. (2014). An open science resource for establishing reliability and reproducibility in functional connectomics. *Scientific Data*, *1*, 140049. https://doi.org/10.1038/sdata.2014.49

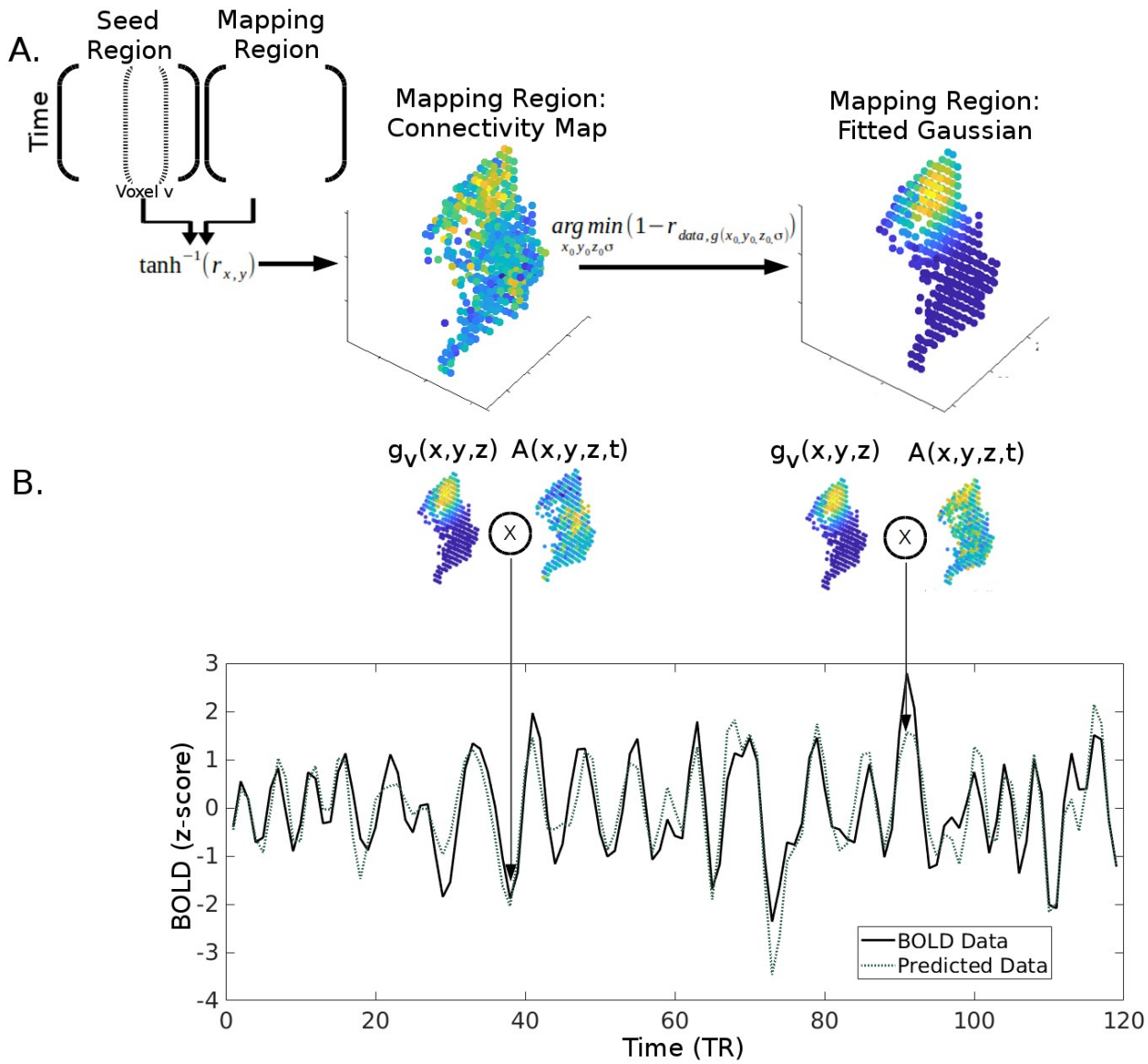

Figure 1: 3D Connective Field Modeling. **(A)** Gaussian fitting procedure. Each seed voxel's timecourse (dotted bracket inside the matrix on the left represents the timecourse of one voxel of the seed region) is correlated to every voxel's timecourse in the mapping region and then Fisher's z transformed. For each seed voxel, the corresponding 3-D Fisher's Z matrix is then fitted to the 3 dimensional Gaussian model, by minimizing the correlation distance between the Fisher's Z matrix and the Gaussian distribution. The fitted Gaussian parameters, location and standard deviation parameters, for each seed voxel are used in subsequent quantitative tests. **(B)** Time-series prediction model. For

each time-point, the overlap between the actual activation in the mapping region [A(x,y,z,t)] and the fitted Gaussian distribution in the mapping region [g_v(x,y,z)] for that particular seed voxel produce the expected level of activity in the corresponding seed voxel. The first arrow points to a period of low overlap, and thus a period of low expected level of activity, while the second arrow points to a period of high overlap, and thus a period of low expected level of activity. This procedure was used to evaluate the performance of the 3-D connective field model.

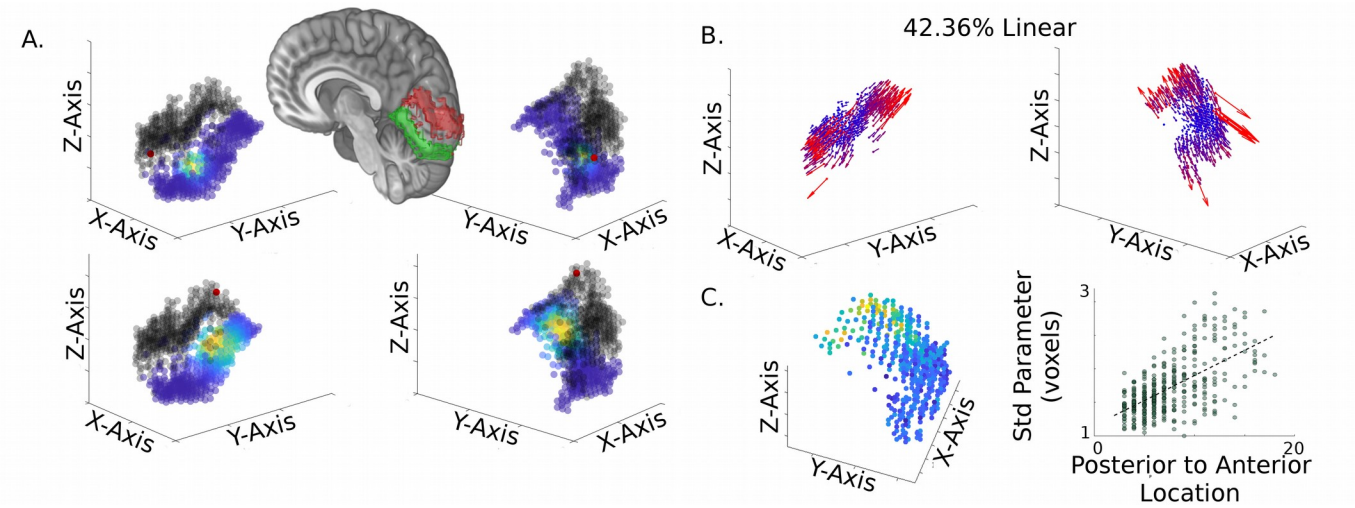

Figure 2: Group results of the 3-D connective field modeling in dorsal and ventral visual cortex using the Cambridge Buckner resting-state fMRI dataset. **(A)** Examples of the resulting Gaussian model are shown for two seed voxels (red dots), plotted in red among other voxels (black circles) in dorsal visual cortex (red masked area in the right hemisphere), and their associated group level Gaussian fit (color scale ranged from blue to yellow) in ventral visual cortex (green masked area). For full visualization, each two column shows two plots of the seed voxel's fitted map rotated by 180 degrees from each other. Full animation can be found in Supplementary materials. **(B)** Preferred location of connectivity of each seed voxel is plotted as a vector with the origin in the seed location, and the vector direction showing the fitted x_0 y_0 and z_0 parameters. The vectors are colored coded with blue to red representing low to high euclidean norm of the vector. **(C)** Group average of the Gaussian model's standard deviation parameter. Left, each voxel within the seed region, dorsal visual cortex, is plotted with the data point's color scaled by the standard deviation parameter of their connective field model. Cooler to warmer colors represent smaller to larger standard deviations. Right, this plot shows the correlation between the anterior-posterior extent of the seed voxel and their associated standard deviation parameter, suggesting that standard deviation increases along more anterior voxels.

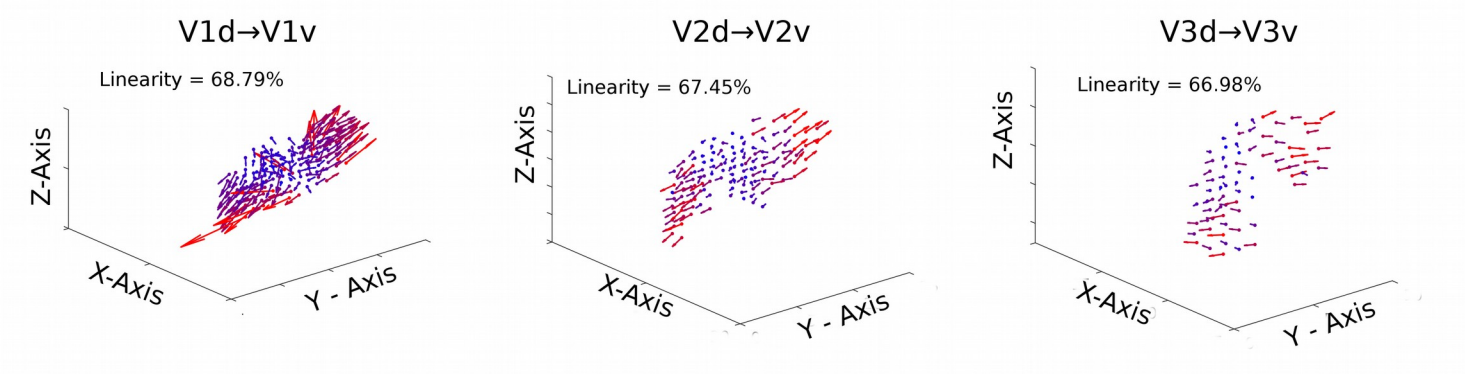

Figure 3: The linear organization pattern of region-to-region functional connectivity is similar across early visual areas. More constrained ROI masks were selected to demonstrate that the connectivity patterns from dorsal to ventral portions of V1, V2, and V3 are constrained by the anterior-posterior axis, likely along the topographic eccentricity representation. The vector fields are displayed similarly as described in Figure 2, with the red-blue color scale representing the euclidean norm of each seed voxel's vector.

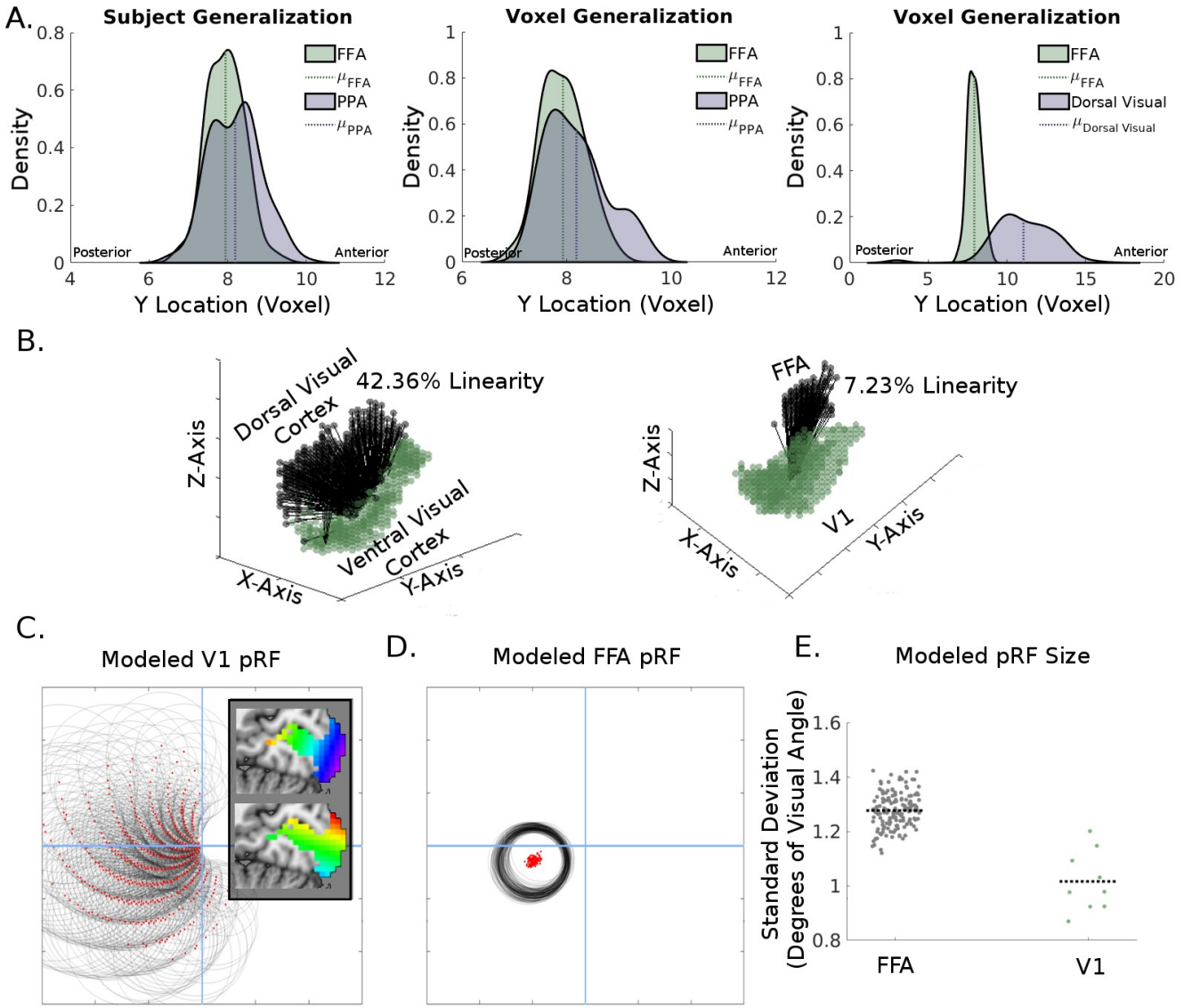

Figure 4: Pattern of functional connectivity between FFA and V1 corresponds well with FFA's more central/foveal pRF observed in previous studies. **(A)** As shown across subjects (left) and across voxels (middle), compared to the PPA, FFA showed a more posteriorly located and narrower range of connectivity with V1. For comparison, the rightmost plot shows the distribution of Y Location parameters for the FFA to V1 model is as well as the dorsal visual cortex to ventral visual cortex model. **(B)** Another representation of the biases of FFA to V1 connectivity (right) in comparison to dorsal and ventral visual cortex connectivity (left). The black points represent voxels within the seed region and

the green points represent voxels within the mapping region, with the vectors connecting them represent the seed voxels' preferred connectivity location along the mapping region. Note the relatively higher amount of convergent connectivity from FFA to V1 and much lower linearity. **(C)** Using an ideal model of V1 organization, with 2 orthogonal axes representing eccentricity and angle (see inset), we show that applying the group fitted region to region pRF mapping of V1 from FFA, we can reproduce some important qualities of FFA's pRF, such as a more central representation **(D)** and quantitatively larger pRFs **(E)**. Plots shown in **(C,D)** are visualized similarly as in previous studies (Kay et al., 2015) with red dots representing the center of the pRFs and the gray circles representing the standard deviation of the pRFs, plotted on the 4 quadrants of visual space. As the ROIs are in the right hemisphere, the pRFs of the seed voxels show lateralized representation of the left visual space.

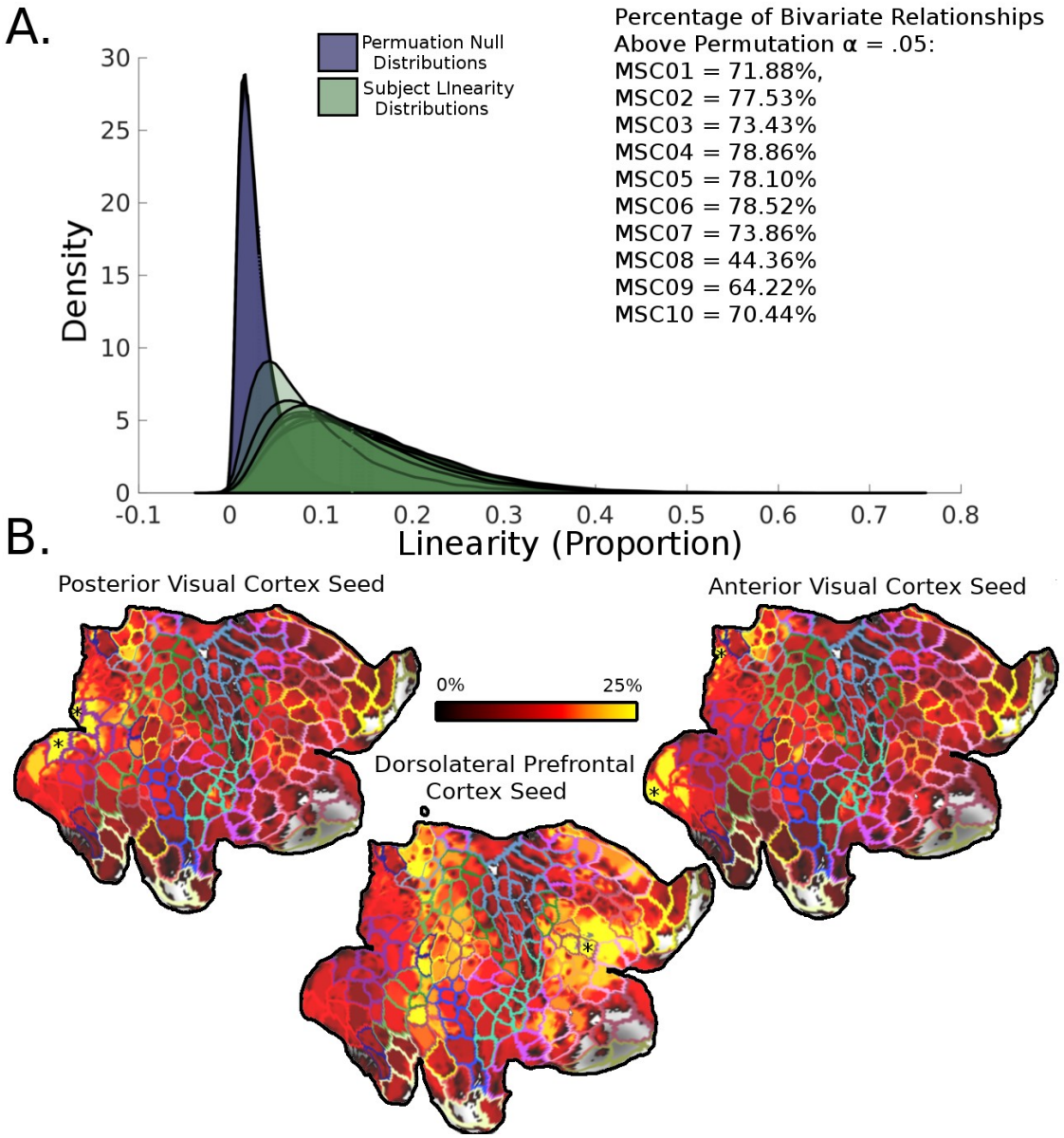

Figure 5: Linearity of input as a general rule of functional connectivity between cortical regions. **(A)** Each MSC subject's distribution of linearity estimates is plotted against their own permutation null distribution. All subjects showed a large proportion of bivariate relationships that are of greated linearity than would be expected due to chance. **(B)** Mean linearity estimates are shown from 3 seed regions (shown as * in each map), posterior visual cortex, anterior visual cortex, and dorsolateral prefrontal cortex. The color scale from darker to brighter color represents lower to higher linearity for the seed regions' connective field in the other brain regions. This whole brain illustration demonstrates

that while linearity is a general phenomenon for region-to-region connectivity, it is maintained within specific networks, suggesting function in maintaining integrity of information transfer across regions within a network.

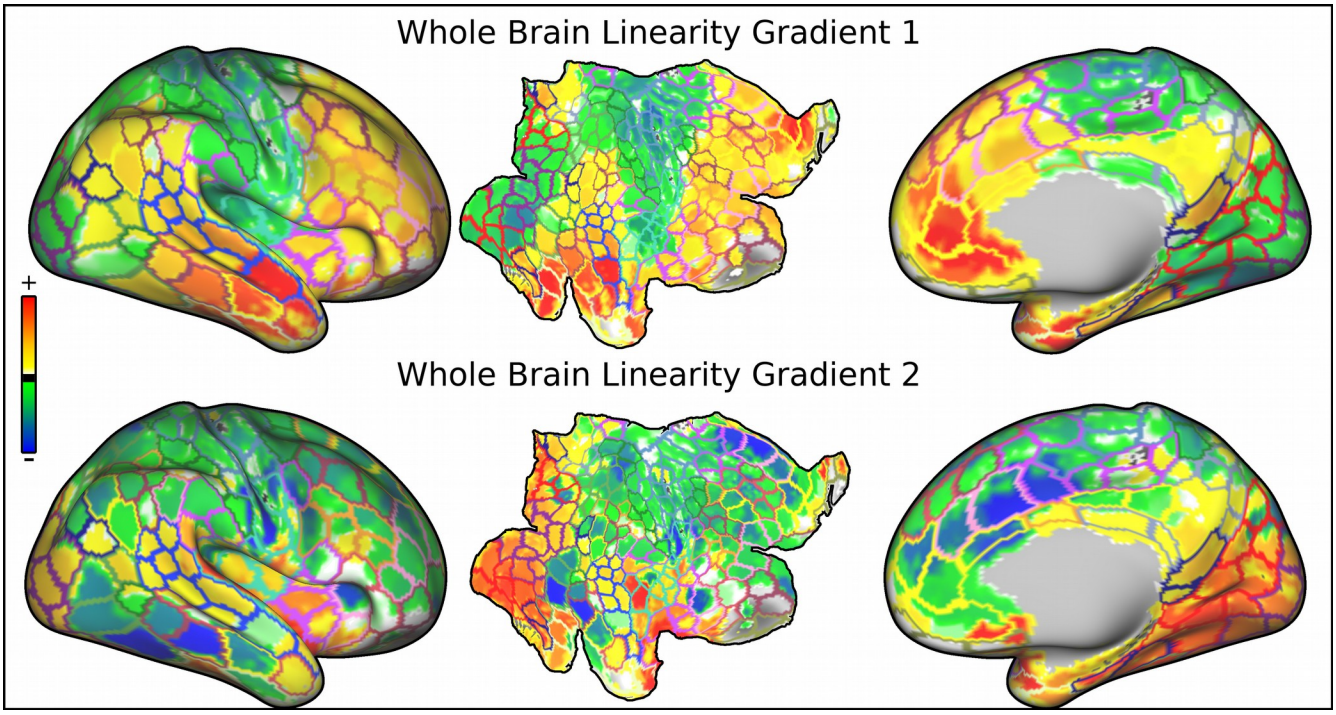

Figure 6: Gradient decomposition of whole brain linearity. Whole brain region-to-region linearity matrix was decomposed using nonmetric multidimensional scaling in order to examine organizational patterns of linearity across the brain. The gradients are color scaled from red to blue, with red-yellow colors representing one side of the gradient, and blue-green colors representing the other side of the gradient. **(TOP)** First whole brain linearity gradient, demonstrates a segregation of unimodal sensory areas and multimodal association areas. **(BOTTOM)** Second whole brain linearity gradient, the fractionated nature suggests potential integration of information across unimodal sensory areas and multimodal association areas.

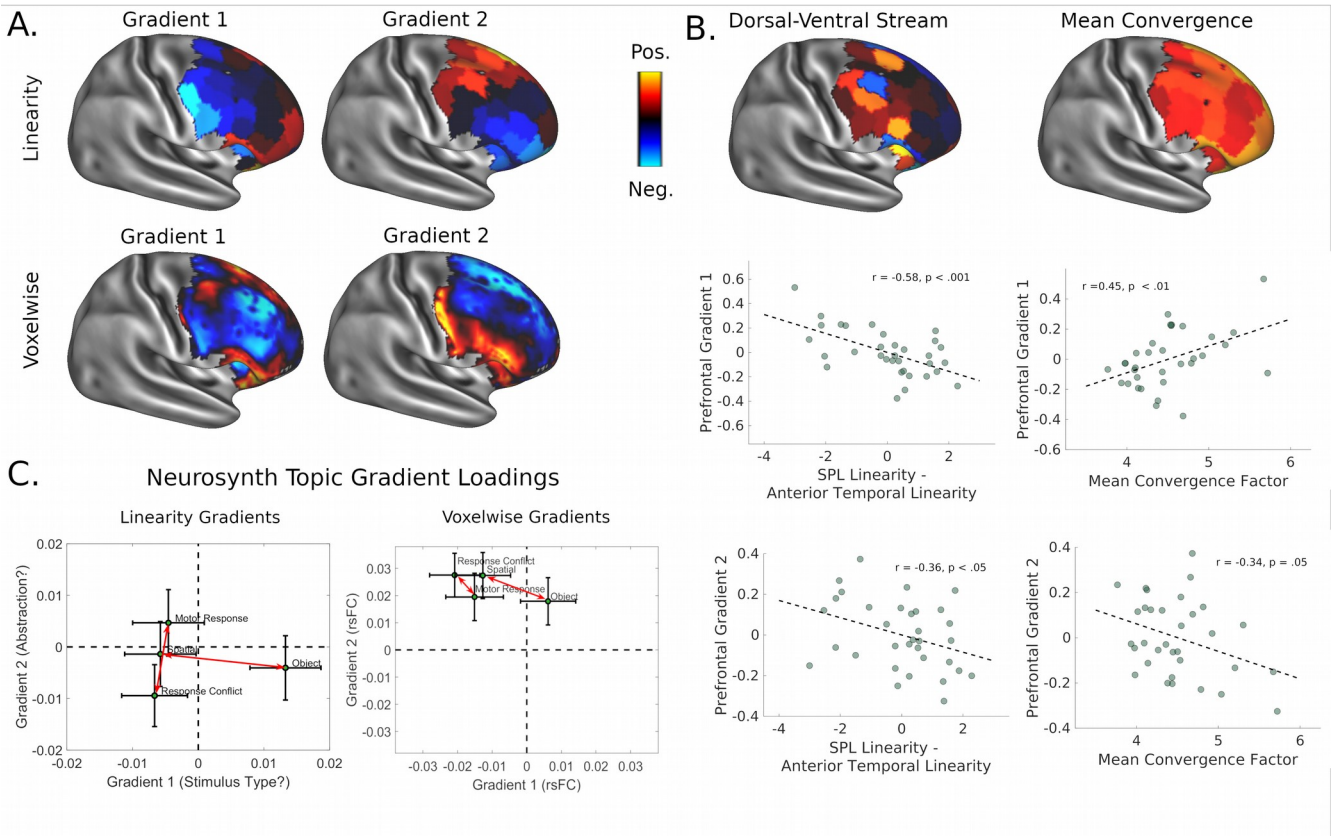

Figure 7: Decomposition of functional connectivity within lateral prefrontal cortex. **(A)** The decomposition of the bivariate linearity of the lateral prefrontal cortex revealed two gradients. Gradient 1 demonstrates an organization from posterior middle frontal gyrus/inferior precentral sulcus to anterior inferior frontal gyrus/frontopolar cortex, while Gradient 2 demonstrates an organization from posterior superior frontal cortex to anterior inferior frontal gyrus. Gradients produced from conventional voxelwise resting state functional connectivity (rsFC), however, simply segregate middle frontal gyrus and inferior frontal gyrus from the rest of the prefrontal cortex, respectively. **(B)** We examined the correlates to the gradient organization derived from linearity, particularly the differential linearity from dorsal and ventral stream regions, and the average convergence factor of each prefrontal parcel with all other prefrontal parcels. Top brain images display these factors within the prefrontal cortex, while the bottom images shows the zero order correlations between these factors and the linearity gradients. **(C)** Relating the modeling results to mainstream theories of prefrontal functional

organization. Using Neurosynth meta-analyses as masks, we examined the gradient loadings on 4 topics (spatial, object, motor response, response conflict) related to the two dominate organizational frameworks of the prefrontal cortex. Plotted on the left are the mean linearity gradient values (and their standard error to the mean) for each of these topics, while on the right are the mean voxelwise connectivity gradient values (and their standard error to the mean). Red arrows connect the terms that should be theoretically segregated. Important to note the relative orthogonality of the red arrows in the linearity gradient plot.

Table 1: Regression Analysis on Lateral Prefrontal Gradients

Gradient 1 Analysis				
	Beta	Standard Error	T-value	P-value
Intercept	0.000	0.130	0.000	1.000
D-V Linearity	-0.534	0.152	-3.512	0.001
Convergence	0.390	0.152	2.567	0.016
Linearity	-0.021	0.172	-0.120	0.905
Gradient 2 Analysis				
	Beta	Standard Error	T-value	P-value
Intercept	0.000	0.156	0.000	1.000
D-V Linearity	-0.350	0.182	-1.922	0.064
Convergence	-0.418	0.182	-2.300	0.029
Linearity	-0.092	0.205	-0.446	0.659